RSC Advances

ROYAL SOCIETY OF CHEMISTRY

www.rsc.org/advances

Improving photovoltaic performance of dye sensitized solar cells based on a hierarchical structure with up/down converter

School of Physics and Technology, University of Jinan, Jinan 250022, Shandong Province, P R China

Nannan Yao, Jinzhao Huang*, Ke Fu, Xiaolong Deng, Meng Ding, Shouwei Zhang, Xijin Xu*

*Corresponding author. E-mail address: jzhuangjz@hotmail.com(J. Huang) ; sps_xuxj@ujn.edu.cn(X. Xu)

Abstract

A hierarchical structure combined of porous TiO_2:Al_2O_3:Eu^{3+} nanoparticles (NPs) and vertically grown one-dimensional TiO_2:Er^{3+},Yb^{3+} nanorods (NRs) on fluorine doped tin oxide (FTO) substrates coated with a TiO_2:graphene (G) seed layer was investigated as photoanode for dye sensitized solar cells (DSSCs). The DSSCs assembled with the hierarchical structure exhibit an outstanding power conversion efficiency of 4.58%, which is superior to that of the devices based on pure TiO_2. This high performance can be attributed to the spectrum modifications by utilizing the upconversion (UC) material TiO_2:Er^{3+},Yb^{3+} and downconversion (DC) material Al_2O_3:Eu^{3+}, which facilitates the light harvesting of solar cells via converting near infrared (NIR) and ultraviolet (UV) radiation to visible emission respectively. Also TiO_2:G layer provides a faster electron transport from TiO_2 to FTO for the high carrier mobility of G. Moreover, one-dimensional nanorod structure can offer direct electrical pathways for photogenerated electron as well as enhance the light scattering capabilities of photoanodes. This work indicates that TiO_2:G/TiO_2:Er^{3+},Yb^{3+} NRs/ TiO_2:Al_2O_3:Eu^{3+} hierarchical structure has the potential to improve the performance of DSSCs.

1. Introduction

With the development of society, the fossil fuels are excessive exploited, which

have been causing the world energy crisis and environmental pollution. Renewable energy utilization is an effective solution for the world energy crisis and environmental pollution. Dye sensitized solar cells (DSSCs) have received renewed interest as a renewable energy source for their low cost, easy fabrication procedures, safe non-toxic, showing great advantages and broad application prospects [1,2]. In general, DSSCs are a type of photoelectrochemical system consisting of a porous nanocrystalline TiO_2 film sensitized by dye for absorbing incident light, a redox electrolyte, and a platinum counter electrode acts as catalyst for redox couple regeneration reaction [3]. Considerable efforts have been devoted to the DSSCs over the past decade [4-7]. However, the conversion efficiency of DSSCs is still limited by many factors, such as electron injection efficiency, light harvesting efficiency, as well as the rate of charge recombination [8,9,10].

The TiO_2 nanocrystalline deposited on conductive substrate fluorine doped tin oxide (FTO) as photoanode of DSSCs plays a significant role in the light harvesting and the transfer of photoinduced carrier [11,12]. To date, the highest efficiency of DSSCs has reached to 13 % with porous TiO_2 film [13]. The usual porous nanocrystalline TiO_2 film offers a high surface area to absorb enough dye. However, the porous structure is not in favor of electron transport due to the multiple transport paths among different grain boundaries [14]. One-dimensional nanostructure such as nanorod or nanotube arrays have been adopted to address this issue by providing direct electrical pathways for electrons along the direction of the nanorod and increased electrons lifetime [15-17]. It is noteworthy that one-dimensional TiO_2 nanostructure alone grown on substrate has an insufficient exposed surface area for the adsorption of dye [18]. Therefore, we use a composite structure containing TiO_2 nanorods (NRs) and nanoparticles (NPs) as photoanode to solve the issue existed in each case.

In DSSCs, the most conventionally used Ruthenium dyes such as N719 usually absorb light only in visible range due to the relatively large optical bandgap of 1.8 eV, resulting in a lot of energy losses in ultraviolet and infrared region [19,20]. An effective way to avoid the loss of photo energy is the utilization of upconversion (UC)

or downconversion (DC) materials, which aim to shift the incident solar spectrum to better match the absorbed spectrum of the dye so as to enhance conversion efficiency of the solar cells [11,21,22]. Lanthanide ions are often used as UC or DC luminescence centers due to their intra 4f transitions [23]. Photon UC is a process in which the sequential absorption of two or more low energy photons leads to the emission of a high energy visible photon [24]. Lanthanide ions of Er^{3+}, Ho^{3+}, Tm^{3+}, Pr^{3+}, Tb^{3+} have attracted much attentions for the investigation of upconverter, and Yb^{3+} ion is usually co-doped as sensitizer to increase the near infrared (NIR) absorption strength of the upconverter [25]. Among these UC materials, the Er^{3+}/Yb^{3+} couple was the most researched pair until now [26]. In addition, downshifting has also been applied for the improvement of solar cell efficiencies, and Eu^{3+} is the well-studied lanthanide ion for its ultraviolet (UV) absorption and red emission [27].

In this paper, the main idea is to utilize up and down conversion of UV and IR parts of the sun light into the region of dye absorption, as well as use graphene (G) to achieve faster electron transfer, which is efficient to enhance the performance of DSSC. Thus, a multifunctional TiO_2:G/TiO_2:Er^{3+},Yb^{3+} NRs/ TiO_2:Al_2O_3:Eu^{3+} composite structure is applied to construct photoanode of DSSCs. Here, we considered the effect of TiO_2:G compact film between FTO and TiO_2 nanorod arrays. Wang et al. reported that DSSCs based on the TiO_2 nanorod arrays grown on the seeded-FTO substrate have longer electron lifetime, which could reduce the electron recombination and lead to an enhanced performance of the cells [28]. The presence of G facilities the electron transfer to FTO due to its excellent electron mobility at room temperature [29]. What's more, the introduction of TiO_2:Er^{3+},Yb^{3+} NRs can not only benefit electron transport, but achieve light confinement. Also, the UV light can be used by cells through the DC luminescence process of Al_2O_3:Eu^{3+} in TiO_2 paste. Therefore, the performance of DSSCs will be effectively improved.

2. Experimental

2.1 Preparation of TiO_2:G seed layer on the FTO substrate

FTO glasses were used as substrate and pretreated by cleaning ultrasonically in

acetone, ethanol and deionized (DI) water for 20 min in turn, then rinsed with distilled water and lastly dried at 80 °C. To synthesize the TiO_2:G sol, 5 ml tetrabutyl titanate ($Ti(OBu)_4$) was dissolved in 15 ml ethanol and 0.5 ml acial acetic acid, then 0.25 ml nitric acid, 5 ml ethanol and 0.5 ml deionized water were added in the solution. In addition, 20 mg commercial G (XF001W) was also dispersed in the above solution with ultrasonic dispersion for 2 h. The TiO_2:G seed layer was prepared on the FTO substrate by spinning the sol. And then the samples were dried and finally annealed at 500 ^oC for 1 h.

2.2 Synthesis of TiO_2 :Er^{3+}, Yb^{3+} nanorod arrays

The TiO_2 nanorod arrays was prepared using a hydrothermal method reported previously [30]. Typically, 0.5 ml of ($Ti(OBu)_4$) was added in a mix solution of 15 ml DI and 15 ml HCl (38 wt. %) under stiring at room temperature in a Teflon-lined stainless steel autoclave. Moreover, in order to synthesis the TiO_2:Er^{3+},Yb^{3+} nanorods, $Er(NO_3)_3 \cdot 6H_2O$, $Yb(NO_3)_3 \cdot 6H_2O$ were dissolved in the transparent solution with mole ratio of Ti^{4+} to Er^{3+} and Yb^{3+} 1:0.01:0.01 and 1:0.01:0.05 under vigorous stirring at room temperature. After stirring for 30 min, the FTO substrates coated with TiO_2:G seed layer were placed in the Teflon-lined autoclave and heated at 150 °C for 6 h in an electric oven. Then the samples were cooled down to room temperature, followed by rinsing with DI water.

2.3 Synthesis of Al_2O_3:Eu^{3+} NPs

Eu^{3+} doped Al_2O_3 NPs with different doping concentrations (1 mol %, 2 mol % and 3 mol %) were synthesized by precipitation method. $Al(NO_3)_3 \cdot 9H_2O$ and $Eu(NO_3)_3 \cdot 6H_2O$ were dissolved in DI water under vigorous stirring at room temperature, then ammonium hydroxide was added in the transparent solution to adjust pH of 3 (solution a). And NH_3HCO_3 was added in ammonia aqueous solutions to obtain a pH of 10, some PEG acted as dispersant was also added in the solution (solution b). Then saline solution was drip slowly into the above solution b under stirring for 1 h. The precipitate was collected by centrifugation at 5000 rpm and

washed with distilled water several times to remove the excess solvent and impurities. After dring in a hot air oven at 100 °C for 24 h, the obtained brown powder was annealed at 1200 °C for 4 h in a muffle furnace and white powders of Al_2O_3: Eu^{3+} were finally obtained.

2.4 DSSCs assembly

To prepare the TiO_2:Al_2O_3:Eu^{3+} composite film electrodes, 10 mg of Al_2O_3:Eu^{3+} was added in the TiO_2 pastes according to our previous report [27]. The photoanode pastes were prepared by the doctor blade method after the synthesis of TiO_2:Er^{3+}, Yb^{3+} NRs grown on FTO substrates covered by TiO_2:G layer. And then, the TiO_2:G/TiO_2:Er^{3+},Yb^{3+} NRs/ TiO_2:Al_2O_3:Eu^{3+} hierarchical structure was annealed at 450 °C for 30 min. After cooling down to 80 °C, in order to absorb the dye, the photoelectrodes were immersed into an ethanol solution of 0.36 mM N719 ruthenium dye for 24 h at room temperature, finally washed with ethanol to remove the nonchemisorbed dye and dried in air. Pt (OPV-Pt-S) electrode was prepared by spin-coating method and annealed at 450 °C for 30 minutes. Subsequently, fixing the photoanode and Pt counter electrode together by a hot-melt film spacer, followed by injecting electrolyte (OPV-MPN-I) into the space between the electrodes to assemble the DSSCs. Fig.1 shows the fabrication process of DSSCs based on TiO_2:G/ TiO_2:Er^{3+},Yb^{3+} NRs/TiO_2:Al_2O_3:Eu^{3+} hierarchical structure. In this paper, a comparative study of photovoltaic performance of DSSCs with different photoelectrodes was carried out. The photoelectrodes structures of DSSCs as follows: TiO_2/TiO_2 NRs/TiO_2, TiO_2:G/TiO_2 NRs/TiO_2, TiO_2:G/TiO_2 NRs/TiO_2:Al_2O_3:Eu^{3+} and TiO_2:G/TiO_2:Er^{3+},Yb^{3+} NRs/TiO_2:Al_2O_3:Eu^{3+}.

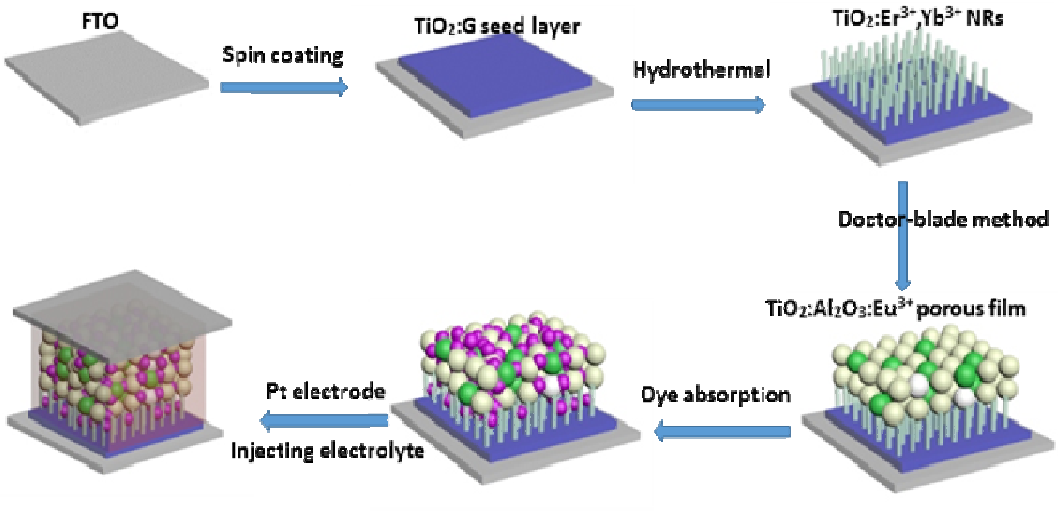

Fig. 1 The fabrication process of DSSCs based on TiO_2:G/TiO_2:Er^{3+},Yb^{3+} NRs/TiO_2:Al_2O_3:Eu^{3+} hierarchical structure

2.5 Characterization

The structure of the Al_2O_3:Eu^{3+} and TiO_2:Er^{3+}, Yb^{3+} was investigated by X-ray diffraction (XRD, D8-Advance, Bruker). The photoluminescence (PL) of samples was measured using the 7-FRSpec fluorescent spectrometer made by Sofn using a Xe lamp as the excitation source. The surface and cross-section morphology of photoanode structures were examined with field emission scanning electron microscope (FE-SEM, Quanta FEG250). The photocurrent response to time and the transient open-circuit potential measurements were performed by cycles of light switching on and off under a Xe lamp as the light source. The absorption spectrum of composite electrodes sensitized by N719 was tested to confirm the effectiveness of converters. And the incident-photon-to-current-conversion efficiency (IPCE) measurement was carried out in a standard three-electrode system with 1 M NaOH aqueous solution as supporting electrolyte, in which composite structures coated on FTO, platinum wire and Ag/AgCl act as the working electrode, counter electrode electrode and the reference electrode, respectively. The I–V characteristics of the DSSCs were measured with an Aglient B2901A source/meter under a Xe lamp. The irradiation areas of the working electrode were about 0.16 cm^2. All these

measurements were conducted at room temperature.

3. Results and discussion

As shown in Fig.2, the crystal structures of $Al_2O_3:Eu^{3+}$ and $TiO_2:Er^{3+},Yb^{3+}$ can be confirmed by XRD. From the XRD patterns of $Al_2O_3:Eu^{3+}$ powder (Fig.2.(a)) and $TiO_2:Er^{3+},Yb^{3+}$ NRs grown on FTO (Fig.2.(b)), the main diffraction peaks are indexed to Al_2O_3 (JCPDS No. 86-1410) and rutile phase TiO_2 (JCPDS No. 21-1276) respectively, and no diffraction peaks related to other oxide phases are observed, indicating that rare earth ions might have been incorporated into Al_2O_3 and TiO_2 lattice. In Fig.2.(a), the broad and low intense peaks indicate the smaller size of the particles. And it is observed that the $TiO_2:Er^{3+},Yb^{3+}$ crystal growth is (004)-oriented and shows well crystallinity in Fig.2.(b).

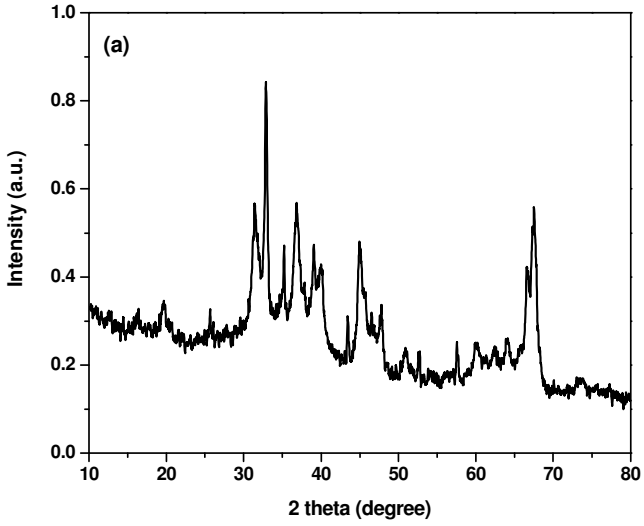

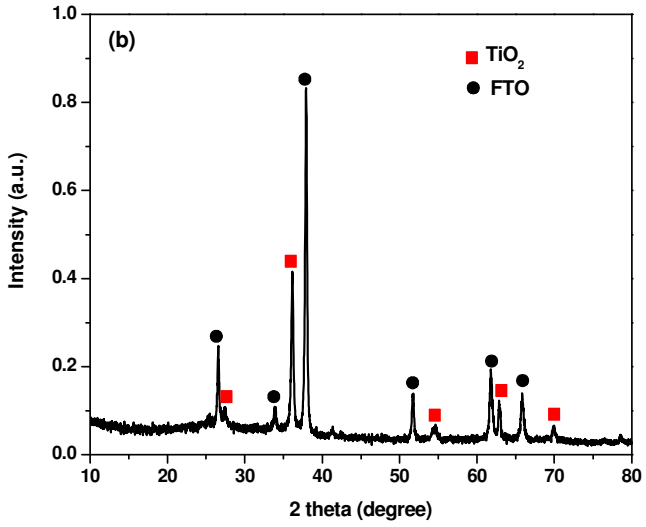

Fig. 2 XRD patterns of (a) $Al_2O_3:Eu^{3+}$ power and (b) $TiO_2:Er^{3+},Yb^{3+}$ NRs grown on FTO

The room temperature PL spectra of $Al_2O_3:Eu^{3+}$ and $TiO_2:Er^{3+},Yb^{3+}$ have been carried out to illustrate the DC and UC process, respectively. The emission spectrum of $Al_2O_3:Eu^{3+}$ under 320 nm excitation is presented in Fig.3.(b). A fact that Eu^{3+} emission is observed under UV (320 nm) excitation, which is not absorbed by Eu^{3+}. Thus, the dopant is excited indirectly by effective energy transfer from Al_2O_3 to Eu^{3+}. In Fig.3.(b), the most intense and sharp emission peak in the red spectral region was observed in $Al_2O_3:Eu^{3+}$, and the emission peaks at 577 nm, 590 nm, 598 nm, 617 nm and 653 nm can be attributed to the $^5D_0$-^7F_J transitions (J=0-3) of Eu^{3+}. Also, a weak broad emission around 400 nm-450 nm could be related to the intrinsic defect emission in the Al_2O_3 host. The inset in Fig.3.(b) shows PL spectrum of $Al_2O_3:Eu^{3+}$ with different doping concentrations. It is obvious that the PL intensity of Eu^{3+} decreased following the increased Eu^{3+} concentration.

The PL spectrum of Er^{3+}, Yb^{3+} co-doped TiO_2 was obtained with the excitation of 980 nm laser. For the $TiO_2:Er^{3+}$, Yb^{3+}, Er^{3+} act as activator and Yb^{3+} has been demonstrated as sensitizer with a absorption of 980 nm corresponding to the $^2F_{5/2}$-$^2F_{7/2}$ transition. The visible luminescence spectrum of TiO_2: Er^{3+}, Yb^{3+} shown in Fig. 3.(c)

reveals two emission bands in the green and red spectral regions due to the intra-4f transitions of rare earth ions and the PL intensity is TiO_2:1 mol % Er^{3+}, 1 mol % Yb^{3+}>TiO_2:1 mol % Er^{3+}, 5 mol % Yb^{3+} in the inset. The green emission bands observed between 520 nm and 550 nm correspond to $^2H_{11/2}$-$^4I_{15/2}$ and $^4S_{3/2}$-$^4I_{15/2}$ transitions of Er^{3+} ions. The stronger red emission from 650 to 680 nm is attributed to the $^4F_{9/2}$-$^4I_{15/2}$ transition of Er^{3+} ions. It is clear that the NIR light (980 nm) can be shifted to visible light by TiO_2: Er^{3+}, Yb^{3+}. Therefore, in consideration of PL intensity, TiO_2:1 mol % Er^{3+}, 1 mol % Yb^{3+} and Al_2O_3:1 mol % Eu^{3+} were chosen as up/down conversion materials to convert NIR and UV radiation to visible emission respectively, which will reduce the energy loss in ultraviolet and infrared region and broaden the absorption of N719 (Fig.3.(a)).

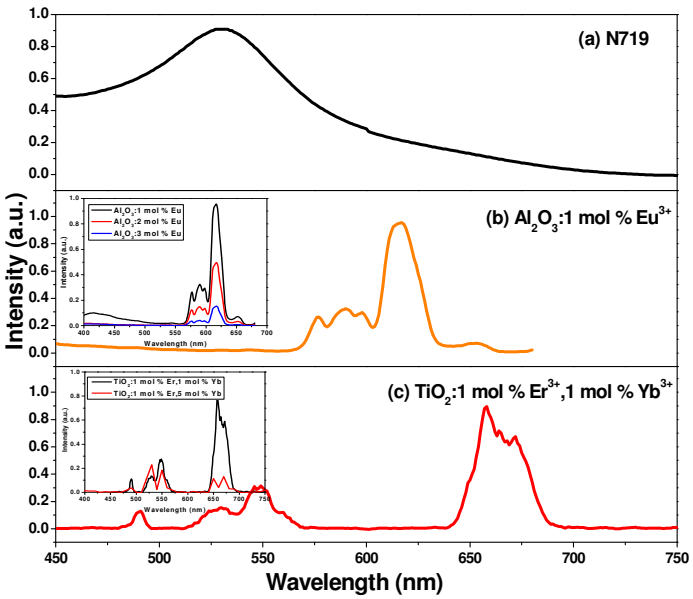

Fig. 3 (a) Absorption of N719; (b) PL spectrum of Al_2O_3:Eu^{3+} (inset: PL spectrum of Al_2O_3:Eu^{3+} with different doping concentrations) and (c) PL spectrum of TiO_2:Er^{3+}, Yb^{3+} (inset: PL spectrum of TiO_2:Er^{3+}, Yb^{3+} with different doping concentrations)

Fig. 4 shows the surface and cross-section SEM images of the as prepared photoanodes FTO/TiO_2/TiO_2 NRs/TiO_2 and FTO/TiO_2:G/TiO_2:Er^{3+},Yb^{3+} NRs/TiO_2:Al_2O_3:Eu^{3+}. From the top view of the photoanode, FTO/TiO_2/TiO_2

NRs/TiO_2 exhibits a uniform surface morphology with high porosity (Fig. 4.(a)), as well as FTO/TiO_2:G/TiO_2:Er^{3+},Yb^{3+} NRs/TiO_2:Al_2O_3:Eu^{3+} film (Fig. 4.(c)). Also, the cross-sectional SEM images of both photoanodes (Fig. 4.(b) and (d)) show that the thickness of the composite films is about 12 µm, while the length of the NRs is 1 µm as shown in the inserts.

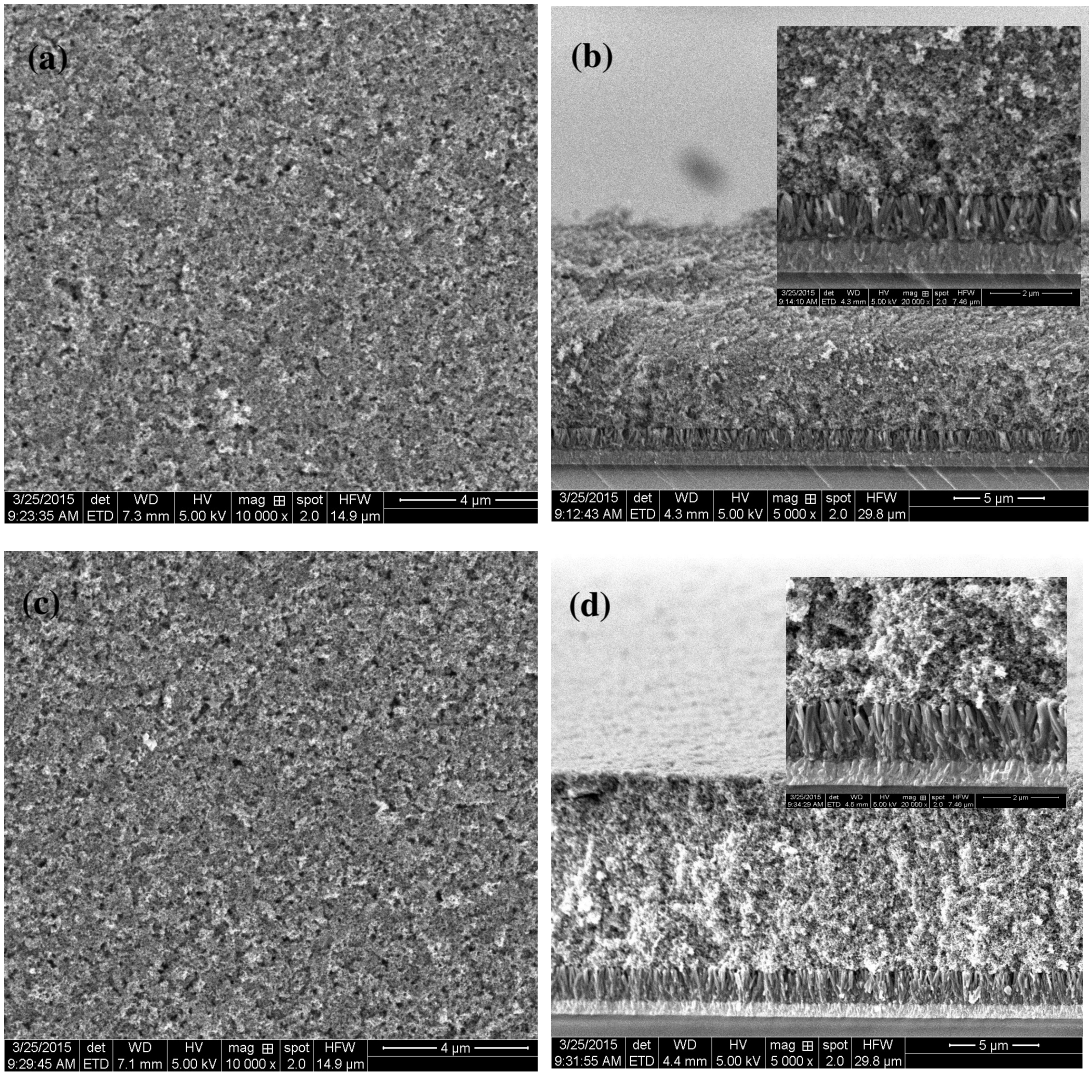

Fig. 4 SEM images of (a) top view and (b) cross-section of FTO/TiO_2/TiO_2 NRs/TiO_2 (the insert of (b) shows higher resolution image); SEM images (c) top view and (d) cross-section of FTO/TiO_2:G/TiO_2:Er^{3+},Yb^{3+} NRs/TiO_2:Al_2O_3:Eu^{3+} (the insert of (d) shows higher resolution image)

The photocurrent response of the samples were examined by the light on-off cycles as shown in Fig.5, which indicate the reproducibility and stability of the photoresponse. From Fig.5, a steady and fast response can be achieved during the light on and off. The photocurrent of samples rapidly increased to a constant value when light was switched on and had a sharp decrease as soon as the light was switched off, indicating a good reproducibility. The trend is repeated with 30 s on-off cycle and shows that all the samples possess a stable photosponse for 200 s under illumination. Obviously, the photocurrent of TiO_2:G/TiO_2:Er^{3+},Yb^{3+} NRs/ TiO_2:Al_2O_3:Eu^{3+} electrode presented a stronger photoresponse than that of other samples under white light. The enhancement in the photocurrent suggests that this composite structure exhibits larger photo-induced electrons and higher transfer efficiency. Therefore, the photocurrent and overall conversion efficiency of DSSCs will be increased efficiently.

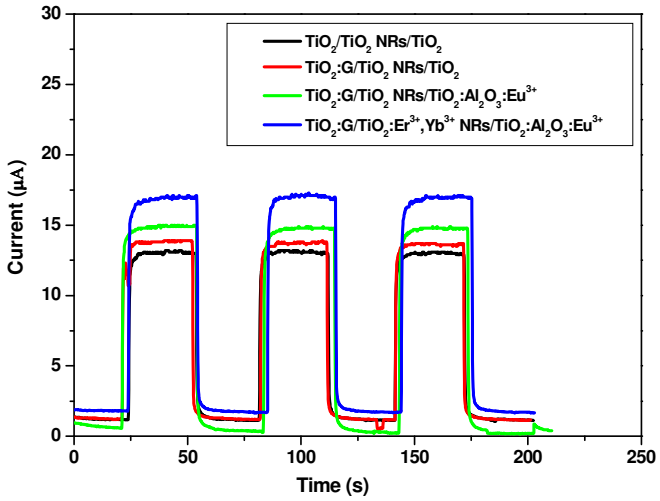

Fig. 5 Photocurrent-time testing curves of TiO_2/TiO_2 NRs/TiO_2, TiO_2:G/TiO_2 NRs/TiO_2, TiO_2:G/TiO_2 NRs/TiO_2:Al_2O_3:Eu^{3+} and TiO_2:G/TiO_2:Er^{3+},Yb^{3+} NRs /TiO_2:Al_2O_3:Eu^{3+}

As for the semiconductor electrode, the photo-induced electronic hole pair will separate and spread to the interface of solution/electrode under illumination,

establishing electric double layer and generating open circuit voltage, which reflects the number of carrier transfering to the surface of the film. Fig.6 shows the transient open-circuit potential of the TiO_2 and TiO_2:G film under the intermittent illumination of Xe light. It's noticed that the TiO_2:G film exhibited a photopotential of 0.065 V, which was larger than TiO_2 film (0.044 V). Enhanced open-circuit potential implied the increasing of carriers in TiO_2:G layer, indicating a faster separation and transport rates of electrons and holes. The slower decay responses of the TiO_2:G compact layer indicates that the recombination is reduced, which was in conformity with the results of the photocurrent response.

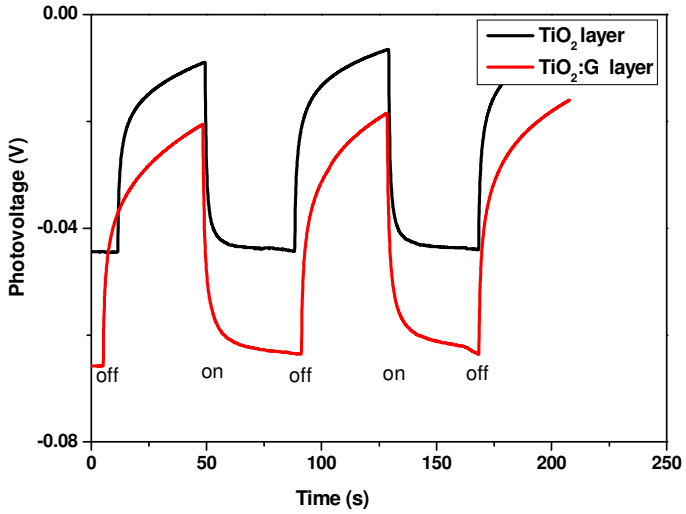

Fig.6 Variation of the open circuit potential of TiO_2 and TiO_2:G film

To confirm the effectiveness of converters, the absorption of photoanodes sensitized by N719 was carried out and the result is presented in Fig.7. It's found that the absorption intensity is enhanced after the incorporation of up/down converter. The TiO_2:G/TiO_2:Er^{3+},Yb^{3+} NRs/TiO_2:Al_2O_3:Eu^{3+} hierarchical structure shows an optimized absorption. For further quantifying the relationship between the photovoltaic performance and the incident light wavelength, the IPCE measurements were conducted on TiO_2/TiO_2 NRs/TiO_2, TiO_2:G/TiO_2 NRs/TiO_2, TiO_2:G/TiO_2 NRs/TiO_2:Al_2O_3:Eu^{3+} and TiO_2:G/TiO_2:Er^{3+},Yb^{3+} NRs/TiO_2:Al_2O_3:Eu^{3+} as shown in

Fig.8. In comparison to pristine TiO_2 electrode, other constructors exhibit higher photon response in visible light region. In addition, the IPCE values of electrodes with the introduction of rare earth ions doped materials was slightly increased in UV light regions due to the increased light absorption, which is agreement with the I-T result.

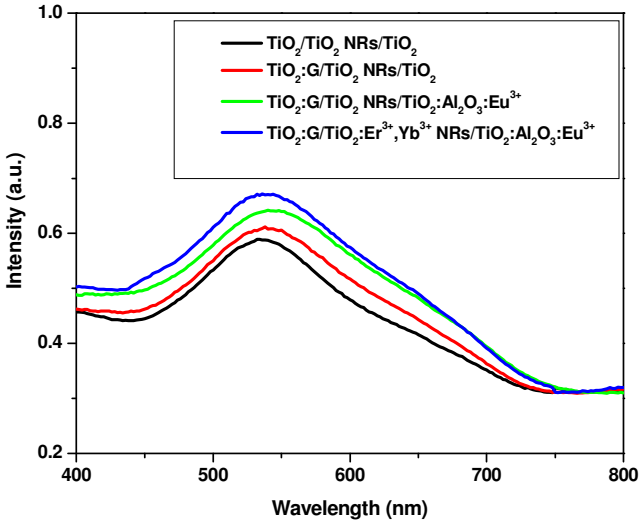

Fig.7 The absorption spectrum of photoanodes sensitized by N719

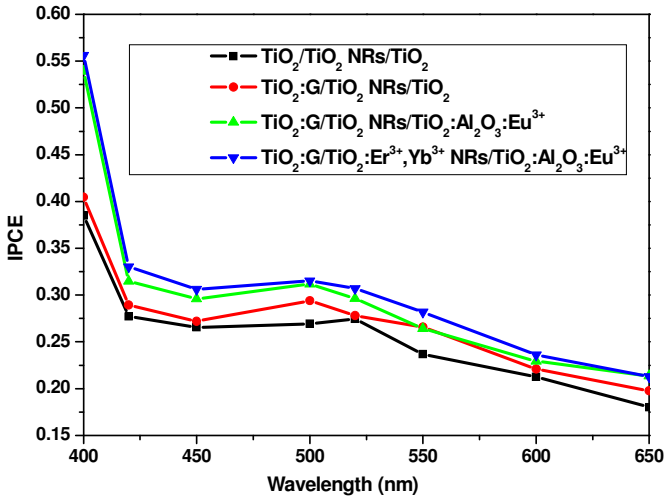

Fig.8 IPCE spectra of TiO_2/TiO_2 NRs/TiO_2, TiO_2:G/TiO_2 NRs/TiO_2, TiO_2:G / TiO_2 NRs/TiO_2:Al_2O_3:Eu^{3+} and TiO_2:G/TiO_2:Er^{3+},Yb^{3+} NRs/TiO_2:Al_2O_3:Eu^{3+}

In order to further verify the influence of G and UC/DC materials, the solar cells based on TiO_2:G/TiO_2:Er^{3+},Yb^{3+} NRs/TiO_2:Al_2O_3:Eu^{3+} hierarchical structure were

fabricated and their photovoltaic performances were investigated. Fig.9. shows the photocurrent-voltage performances of DSSCs with different photoelectrodes. The short-circuit current density (J_{SC}), open-circuit voltage (V_{OC}), fill factor (FF) and the power conversion efficiency (η) of these DSSCs were summarized in Table 1. From the parameters, the cells incorporating TiO_2:G compact layer directly on the FTO glass (TiO_2:G/TiO_2 NRs/TiO_2) has an enhancement of photocurrent and conversion efficiency compared to the cell based on TiO_2/TiO_2 NRs/TiO_2 due to the presence of G, which acted as a charge pathway can reduce the charge recombination rate and enhance the transport of electrons. Also, the DSSCs based on TiO_2:G/TiO_2:Er^{3+},Yb^{3+} NRs/TiO_2:Al_2O_3:Eu^{3+} hierarchical structure have an optimal performance with J_{SC}=10.38 mA cm^{-2} and η=4.58% by utilizing DC and UC materials respectively. It is known that the dye of N719 have a strong absorption around 550 nm. For the Al_2O_3:Eu^{3+}, which can absorb UV light and convert it to visible emission consisted of green and red region. And the NIR light of solar spectrum can be shifted to visible region by TiO_2: Er^{3+}, Yb^{3+} as well. These results have been shown in Fig.3. The effect of DC-luminescence and UC-luminescence, from 600 and 700 nm, is reducing the majority loss of the light in UV and NIR part that the cell without being used. Also, the conversional luminescence, especially the green bands (from 536 to 565 nm) coincide with the best absorption wavelength of the N719. Consequently, UV and NIR irradiation can be absorbed by the N719 dye in the DSSCs through the effect of spectral conversion with the addition of Al_2O_3:Eu^{3+} powder and TiO_2: Er^{3+}, Yb^{3+} NRs in the photoanodes, widening the light absorption range of the cell, thus the light to electricity efficiency will be effectively enhanced.

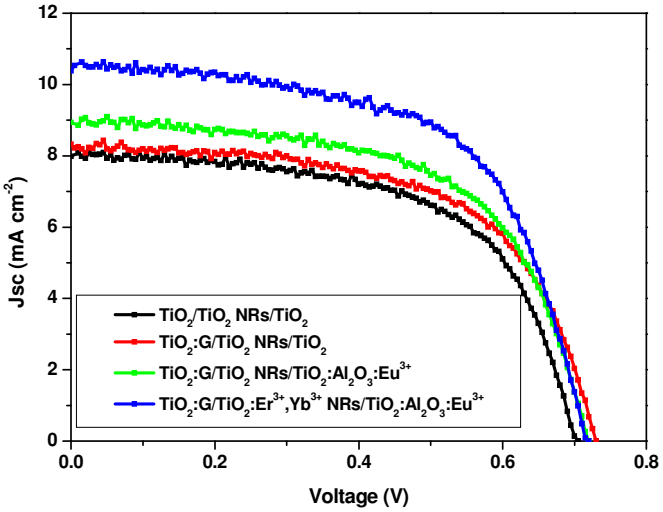

Fig. 9 Photocurrent-voltage curves of DSSCs based on different photoanodes

Table 1. Photovoltaic parameters (short-circuit current density, open-circuit voltage, fill factor, and efficiency) of the DSSCs using different photoelectrode structures

Photoanodes	J_{SC}(mA cm^{-2})	V_{OC}(V)	FF	η(%)
TiO_2/TiO_2 NRs/TiO_2	7.98	0.71	0.60	3.38
TiO_2:G/TiO_2 NRs/TiO_2	8.32	0.73	0.60	3.62
TiO_2:G/TiO_2 NRs/TiO_2:Al_2O_3:Eu^{3+}	8.94	0.72	0.60	3.87
TiO_2:G/TiO_2 :Er^{3+},Yb^{3+} NRs /TiO_2:.Al_2O_3:Eu^{3+}	10.38	0.72	0.61	4.58

Conclusions

In conclusion, a hierarchical structure in the order of TiO_2:G/TiO_2:Er^{3+},Yb^{3+} NRs/TiO_2:Al_2O_3:Eu^{3+} acted as photoanode of DSSCs has been successfully prepared. This hierarchical structure provides a sufficient exposed surface area for the adsorption of dye and direct electrical pathways for photogenerated electron. In addition, the DSSCs based on composite construe possess an excellent capacity to expand light absorption of solar cells via converting UV and NIR radiation to visible

emission by $Al_2O_3:Eu^{3+}$ and $TiO_2:Er^{3+},Yb^{3+}$. And the addition of G into TiO_2 compact film contributes to the increase of short circuit current density due to the faster electron transfer to FTO. Thus, an optimal efficiency of 4.58% was achieved for DSSCs with this hierarchical structure.

Acknowledgements

This work was supported by the National Natural Science Foundation of China (Grant No. 61106059, 11304120, 61504048, 21505050), the Encouragement Foundation for Excellent Middle-aged and Young Scientist of Shandong Province (Grant No. BS2014CL012), the Science-Technology Program of Higher Education Institutions of Shandong Province (Grant No. J14LA01), the Natural Science Foundation of Shandong Provience (Grant No. ZR2013AM008).

References

[1] B. O'Regan and M. Grätzel, *Nature*, 1991, **353**, 737.

[2] M. Grätzel, *Nature*, 2001, **414**, 338.

[3] M. K. Nazeeruddin, E. Baranoff and M. Grätzel, *Sol. Energy*, 2011, **85**, 1172.

[4] K. H. Ko, Y. C. Lee and Y. J. Jung, *J. Colloid Inter. Sci.*, 2005, **283**, 482.

[5] A. Yella , H. W. Lee , H. N. Tsao , C. Yi , A. K. Chandiran , M. K. Nazeeruddin, E. W. Diau , C. Y. Yeh , S. M. Zakeeruddin and M. Grätzel, *Science*, 2011, **334**, 629.

[6] Z. He, W. Que, P. Sun and J. Ren, *ACS Appl. Mater. Inter.*, 2013, **5**, 12779.

[7] G. Li, C. P. Richter, R. L. Milot, L. Cai, C. A. Schmuttenmaer, R. H. Crabtree, G. W. Brudvig and V. S. Batista, *Dalton Trans.*, 2009, **45**, 10078.

[8] Z. He, J. Liu, J. Miao, B. Liu and T. T. Y. Tan, *J. Mater. Chem. C*, 2014, **2**, 1381.

[9] G. B. Shan and G. P. Demopoulos, *Adv. Mater.*, 2010, **22**, 4373.

[10] T. Ganesh, H. M. Nguyen, R. S. Mane, N. Kim, D. V. Shinde, S. S. Bhande, M. Naushad, K. N. Hui and S. H. Han, *Dalton Trans.*, 2014, **43**, 11305.

[11] J. Zhang, H. Shen, W. Guo, S. Wang, C. Zhu, F. Xue, J. Hou, H. Su and Z. Yuan, *J. Power Sources*, 2013, **226**, 47.

[12] A. Sacco, S. Porro, A. Lamberti, M. Gerosa, M. Castellino, A. Chiodoni and S.

Bianco, *Electrochim. Acta*, 2014, **131**, 154.

[13] S. Mathew, A. Yella, P. Gao, R. Humphry-Baker, B. F. E. Curchod, N. Ashari-Astani, I. Tavernelli, U. Rothlisberger, Md. Khaja Nazeeruddin and M. Grätzel, *Nat. chem.*, 2014, **6**, 242.

[14] L. Yang and W. W. F. Leung, *Adv. Mater.*, 2011, **234**, 559.

[15]T. R. Chetia, D. Barpuzary and M. Qureshi, *Phys. Chem. Chem. Phys.*, 2014, **16**, 9625.

[16] L. Li, T. Zhai, Y. Bando and D. Golberg, *Nano Energy*, 2012, **1**, 91.

[17] B. Tan and Y. Wu, *J. Phys. Chem. B*, 2006, **110**, 15932.

[18] H. P. Wu, C. M. Lan, J. Y. Hu, W. K. Huang, J. W. Shiu, Z. J. Lan, C. M. Tsai, C. H. Su and E. W. G. Diau, *J. Phys. Chem. Lett.*, 2013, **4,** 1570.

[19] S. H. A. Lee, N. M. Abrams, P. G. Hoertz, G. D. Barber, L. I. Halaoui and T. E. Mallouk, *J. Phys. Chem. B*, 2008, **112**, 14415.

[20] J. C. G. Bünzli and S. V. Eliseeva, *J. Rare Earth.*, 2010, **28**, 824.

[21] H. Hafez, M. Saif and M. S. A. Abdel-Mottaleb, *J. Power Sources*, 2011, **196**, 5792.

[22] N. Yao, J. Huang, K. Fu, X. Deng, M. Ding, M. Shao and X. Xu, *Electrochim. Acta*, 2015, **154**, 273.

[23] D. Chen, Y. Wang and M. Hong, *Nano Energy*, 2012, **1**, 73.

[24] L. Li, Y. Yang, R. Fan, Y. Jiang, L. Wei, Y. Shi, J. Yu, S. Chen, P. Wang, B. Yang and W. Cao, *J. Power Sources*, 2014, **264**, 254.

[25] H. Lian, Z. Hou, M. Shang, D. Geng, Y. Zhang and J. Lin, *Energy*, 2013, **57**, 270.

[26] H. Yang, F. Peng, Q. Zhang, W. Liu, D. Sun, Y. Zhao and X. Wei, *Opt. Mater.*, 2013, **35**, 2338.

[27] N. Yao, J. Huang, K. Fu, S. Liu, D. E, Y. Wang, X. Xu, M. Zhu and B. Cao, *J. Power Sources*, 2014, **267**, 405.

[28] H. Wang, M. Liu, M. Zhang, P. Wang, H. Miura, Y. Cheng and J. Bell, *Phys. Chem. Chem. Phys.*, 2011, **13**, 17359.

[29] M. J. Allen, V. C. Tung and R. B. Kaner, *Chem. Rev.*, 2009, **110**, 132.

[30] K. Fu, J. Huang, N. Yao, X. Xu and M. Wei, *Ind. Eng. Chem. Res.*, 2015, **54**, 659.

A hierarchical photoanode constructed from G, TiO_2:Er^{3+},Yb^{3+} NRs and Al_2O_3:Eu^{3+} exhibits enhanced efficiency.